Available online at www.sciencedirect.com
ScienceDirect
Journal of the European Ceramic Society 29 (2009) 377–384
www.elsevier.com/locate/jeurceramsoc

Raman spectroscopy, ^{19}F and ^{31}P MAS-NMR of a series of fluorochloroapatites

M.D. O'Donnell [a,b,*], R.G. Hill [a], R.V. Law [b], S. Fong [c]

[a] *Imperial College London, Department of Materials, London, UK*
[b] *Imperial College London, Department of Chemistry, London, UK*
[c] *Atomic Weapons Establishment (AWE), Aldermaston, UK*

Received 9 April 2008; received in revised form 20 May 2008; accepted 17 June 2008
Available online 24 July 2008

Abstract

We report the Raman spectra of a series of fluorochloroapatites $Ca_5(PO_4)_3F_{1-x}Cl_x$, where $x = 0.0$, 0.1, 0.2, 0.4, 0.5, 0.6, 0.8, 0.9 and 1.0 (i.e. from pure fluorapatite to chlorapatite). The series did not appear to exhibit any immiscibility, however peak broadening and additional Raman and NMR spectral features on chlorine addition could be interpreted as reduction in symmetry and ordering in the ion channels. All Raman bands showed significant broadening with chlorine substitution, indicating disordering of the crystal lattice or ordering into fluorine and chlorine rich environments. There was also a general trend of the Raman bands to shift to lower wavenumber linearly with chlorine substitution with the ν_1 phosphate band decreasing from 966 cm^{-1} for $x = 0.0$ to 961 cm^{-1} for $x = 1.0$. The full width half maximum (FWHM) of this band increases linearly with chlorine addition from 5 cm^{-1} for $x = 0.0$ to 10 cm^{-1} for $x = 1.0$. The shift in a component in the ν_3 phosphate band with chlorine addition at around 1035 cm^{-1} agrees with data in the literature on chlorine containing geological apatites. An additional component was seen at around 586 cm^{-1} in the ν_4 phosphate region for chlorapatite and the area of this band decreased linearly to zero as fluorine replaced chlorine. This could be due to E_g symmetry phonons splitting into A_g and B_g modes due to a symmetry change such as hexagonal to monoclinic with chlorine addition. ^{19}F magic angle spinning nuclear magnetic resonance (MAS-NMR) spectra showed a shift to lower ppm values with chlorine addition and a broadening of resonances, consistent with the Raman data. The ^{31}P spectra developed additional shoulders (at around 2 and 4 ppm) with chlorine addition with the main peak position (3.3 ppm for $x = 0$) decreasing for compositions moving away from $x = 0.5$ indicating maximum phosphorous nuclear shielding occurs at an approximate F:Cl ratio of 1:1. This discontinuity is a possible indication of a structural transition at $x = 0.5$ related to local short scale phosphate order ↔ disorder or a change in crystal symmetry.

Keywords: Apatite; Raman; NMR

1. Introduction

Apatite, $Ca_5(PO_4)_3(OH,F,Cl)$, is a predominant component in mineralised tissue such as bone and teeth[1–3] and apatite compounds have numerous applications in fields as diverse as geological dating,[4] optoelectronics,[5] fertilisers,[6] fluorescent lighting[7] and toxic/radioactive waste immobilization.[8,9] The structure of hydroxyapatite, $Ca_5(PO_4)_3OH$, and related materials such as fluorapatite, $Ca_5(PO_4)_3F$, is controversial, complicated by the ease of solid solution and lattice disorder.[10] The Ca(I) site exhibits four-fold symmetry, 4f, and the Ca(II) site six-fold, 6h. OH ions sit in disordered positions above and below the triangles formed by the Ca(II) sites giving rise to the macroscopic space group $P6_3/m$. Fluorine also substitutes onto these sites but in a more ordered manner: in 1/4 and 3/4 positions along the *c*-axis of the unit cell.[11] However, the larger chlorine ion (181 pm compared to 133 pm for fluorine[12]) substitutes in a disordered fashion onto the 0 and 1/2 positions. Pure chlorapatite exhibits a monoclinic structure: $P2_1/b$,[13–15] however in binary and ternary compounds such as $Ca_5(PO_4)_3(F,Cl)$ and $Ca_5(PO_4)_3(F,Cl,OH)$ both monoclinic and hexagonal structures have been observed.[16] It has been noted that this large anion shift

* Corresponding author at: Department of Materials, Imperial College London, Exhibition Road, London, SW7 2AZ, United Kingdom.
Tel.: +44 20 7594 6814; fax: +44 20 7594 6757.
E-mail addresses: m.odonnell@imperial.ac.uk (M.D. O'Donnell), r.hill@imperial.ac.uk (R.G. Hill).

0955-2219/$ – see front matter © 2008 Elsevier Ltd. All rights reserved.
doi:10.1016/j.jeurceramsoc.2008.06.011

in chlorapatite compared to fluorapatite in the tunnels along the 6_3 screw axis with no change in the calcium triad positions possibly limits solid solution behaviour in this system.[11] Chlorine is so displaced from the mirror plane (1.2 Å[17]) an additional bond forms with the Ca(II) changing the calcium coordination. Chlorine does not affect the P–O and Ca(I)–O bond lengths significantly. This large difference in structure of chlorapatie compared to hydroxyapatite and fluorapatite lead researchers to believe the pure compounds would be immiscible and the following adjustments in the structure would therefore be needed to allow solid solution[17]:

- major shifts in the column anion positions,
- a reduction in symmetry, i.e. hexagonal → monoclinic, and/or
- ordering of cations in the individual columns, but disordering of the columns throughout the structure.

Previous diffraction studies[14,15] have show that interactions between F^- and Cl^- results in complex structural features in binary fluorochloroapatites compared to the pure end members.[15] Structural anomalies were attributed to: (i) a trimodal distribution of fluorine sites; in addition to the expected position of fluorine at the centre of the calcium-triads, fluorine is also displaced around 0.2 and 0.6 Å from this position in the *c*-axis ion channels, (ii) an excess of halogen ions per unit cell compared to the stoichiometric total of two and (iii) initial stabilisation of the chlorapatite monoclinic structure with fluorine addition, which destabilised to hexagonal on higher F^- incorporation.[15]

A recent study by McCubbin et al. on a low–OH content fluorochloroapatite[18] by single crystal X-ray diffraction (XRD) and nuclear magnetic resonance (NMR) spectroscopy gave some evidence of short-range monoclinic domains along the *c*-axis but an average macroscopic hexagonal structure.

Although a number of studies have been performed on the structure and properties of binary and ternary apatites in the system $Ca_5(PO_4)_3(OH,F,Cl)$ on geological and laboratory synthesised samples, to our knowledge no authors have performed a complete systematic study on the synthetic series $Ca_5(PO_4)_3F_{1-x}Cl_x$ from $x = 0$ to 1. The purpose of this study is to use Raman microspectroscopy and solid-state nuclear magnetic resonance (NMR) to examine the effect of chlorine addition to fluorapatite on the structure of the mixed compounds and the relation to the pure end members of the series.

2. Experimental

2.1. Material synthesis

A series of fluorochloroapatites of compositions $Ca_5(PO_4)_3F_{1-x}Cl_x$, where $x = 0.0$, 0.1, 0.2, 0.4, 0.5, 0.6, 0.8, 0.9 and 1.0, was synthesised using a solid-state reaction route, by high temperature sintering of the required molar amounts of powdered tricalcium phosphate ($Ca_3(PO_4)_2$), calcium chloride ($CaCl_2$) and calcium fluoride (CaF_2) at around 1000 °C as shown by Eq. (1) for the $x = 0.5$ composition.

$$6Ca_3(PO_4)_2 + CaF_2 + CaCl_2 \rightarrow 2Ca_{10}(PO_4)_6FCl \quad (1)$$

Identification of the final monophase material and confirmation that the reaction had gone to completion was obtained using powder X-ray diffraction (XRD).

2.2. Raman

The Raman system used consisted of a Renishaw RM 2000 spectrometer (Renishaw LC, UK) connected to a Leica microscope with a ×50 objective. A 785 nm 300 mW line focus laser with 100 mW power at the sample was used. This wavelength and 50% power was sufficient to produce a high signal to noise ratio Raman spectrum. The laser spot size was calculated to be 10 μm wide × 20 μm high and 40 μm deep. The spectrometer was set up with a spectrometer slit of 50 μm and 8 CCD (charge-coupled device) pixels. The powdered samples were placed on a glass slide and to collect the spectra five 10 s spectra were taken between Raman wave number shifts of 100 and 1300 cm^{-1}. Quartz was used as a calibration material with the main Raman resonance peak at around 521 cm^{-1}. Overlapping peak positions, areas and widths were obtained by Lorentzian deconvolution in Microcal Origin 6.0 software.

2.3. NMR

The magic angle spinning (MAS)-NMR spectra were recorded using a Bruker DSX 200 MHz spectrometer (4.7 T). Samples were spun in a 4 mm zirconia rotor. ^{19}F spectra were taken at a resonant frequency of 188.29 MHz, using a 10 s delay time and spinning at 10 kHz at the magic angle (54.7°). The ^{19}F spectra were referenced to CaF_2 taken at −108 ppm, relative to the more common standard of $CFCl_3$ and the background was carefully subtracted. ^{31}P spectra were run at a resonant frequency of 81.01 MHz, with a 2 s delay time and spinning at 5 kHz. The reference materials used was 85% H_3PO_4 for ^{31}P and the chemical shift was adjusted to 0 ppm. Peaks were identified and Gaussian deconvolution performed using Microcal Origin 6.0 software.

3. Results and discussion

3.1. Raman

3.1.1. General observations

Fig. 1 shows the Raman spectra of the series $Ca_5(PO_4)_3F_{1-x}Cl_x$. The bands observed for all samples, summarised in Table 1, are consistent with those observed by Penel et al.[19] in fluorapatite. There is a general linear shift to lower wavenumber of all bands with chlorine addition. Fluorapatite ($x = 0.0$) belongs to the $P6_3/m$ (C_{6h}) space group. Theoretical calculations predict the following bands for this space group: five for ν_3 and ν_4, three for ν_2 and two for ν_1[19] which is close to the observed data in Table 1. The mixed

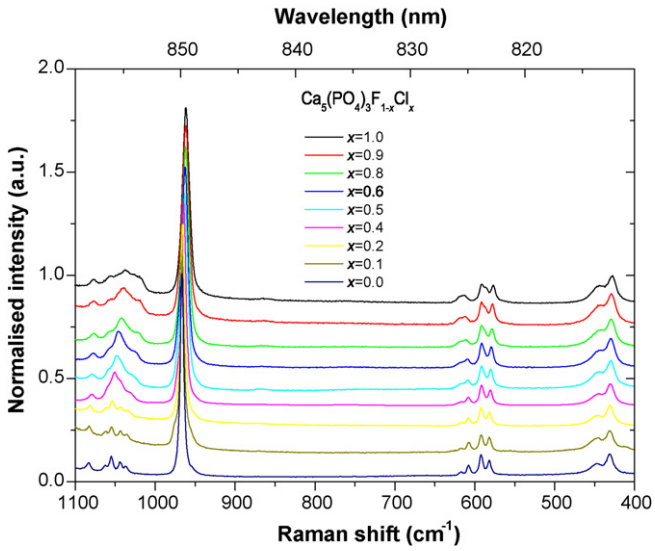

Fig. 1. Raman spectra of the series $Ca_5(PO_4)_3F_{1-x}Cl_x$.

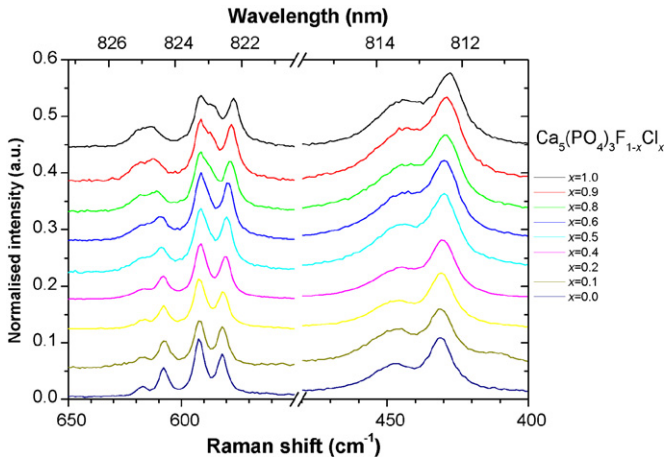

Fig. 2. Raman spectra of ν_2 and ν_4 PO_4^{3-} bands in the series $Ca_5(PO_4)_3F_{1-x}Cl_x$.

compounds should not exhibit $P6_3$ (C_6) symmetry. Due to ionic substitution only the C_3 axis is preserved (the calcium triads). In this scenario, coupling of the modes due to the phosphate groups on the 1/4 and 3/4 planes should be lost and we should then observe 12 bands for the ν_3 and ν_4 modes, 8 for ν_2 and 4 for ν_1. The ionic substitution of Cl^- for F^-, where the mirror plane seen in the pure compounds is lost and should result in a structural transition from hexagonal to monoclinic structure; the compositional point at which this occurs is controversial. This reduction in symmetry will have a minimal effect on non-degenerate phonons. Only degenerate E_g phonons will become A_g and B_g phonons on reduction of symmetry, which will be discussed further below in relation to specific spectral features.

In terms of a classical model, the frequency of a Raman band is dependent on lattice vibrations, the masses of the atoms/ions present and the strength of the forces between the atoms/ions define the position of the vibration. The frequency of the vibration, f, can be described classically by a harmonically oscillating ball and spring model, shown in Eq. (2), known as the Szigeti relationship.

$$f = \frac{1}{c}\sqrt{\frac{k}{\mu}} \tag{2}$$

where c is the velocity of light in a vacuum ($2.998 \times 10^8\ m\,s^{-1}$), k the bond force constant (typically in $N\,m^{-1}$), and μ the reduced mass of the two bonding atoms, two bonding atoms, m_1–m_2 (equal to $m_1m_2/[m_1 + m_2]$). Chlorine is heavier than fluorine (35.45 and 19.00 g mol^{-1}, respectively[12]) and the Ca–Cl bond is weaker than the Ca–F bond (410 and 527 kJ mol^{-1}, respectively[20]). Referring to Eq. (2), chlorine incorporation into the apatite lattice will have the effect of shifting vibrational bands to lower frequencies, as seen in Fig. 1 and Table 1, due to the higher μ and lower k of Ca–Cl.

The entire series appears to be monophase indicating complete miscibility which contradicts previous studies which indicate mixed F–Cl apatite exhibit limited solid solution due to the size difference, different space groups and crystallographic sites of the anions.[11] However, evidence of immisibility cannot be completely eliminated as peak broadening could be due to two similar phosphate chemical environments in fluorine-rich and chlorine-rich ion channels.

Table 1
Position of Raman bands in cm^{-1} for the series $Ca_5(PO_4)_3F_{1-x}Cl_x$, N/A indicates no peak present

PO_4^{3-} band	Cl (x)								
	0.0	0.1	0.2	0.4	0.5	0.6	0.8	0.9	1.0
ν_3	1084	1083	1082	1079	1079	1077	1077	1076	1076
ν_3	1063	1061	1060	1059	1057	1057	1056	1056	1055
ν_3	1055	1055	1053	1050	1048	1046	1042	1040	1038
ν_3	1045	1044	1044	1043	1042	1038	1033	1030	1026
ν_3	1037	1035	1035	1031	1029	1026	1023	1020	1020
ν_1	966	966	965	964	963	962	962	961	961
ν_4	617	616	616	616	617	617	618	618	619
ν_4	608	608	608	608	609	609	611	613	613
ν_4	592	592	592	591	591	591	591	591	591
ν_4	N/A	N/A	591	590	590	588	588	587	586
ν_4	582	582	582	580	580	580	579	578	577
ν_2	447	445	446	445	444	443	441	443	444
ν_2	431	432	431	431	430	430	430	429	428

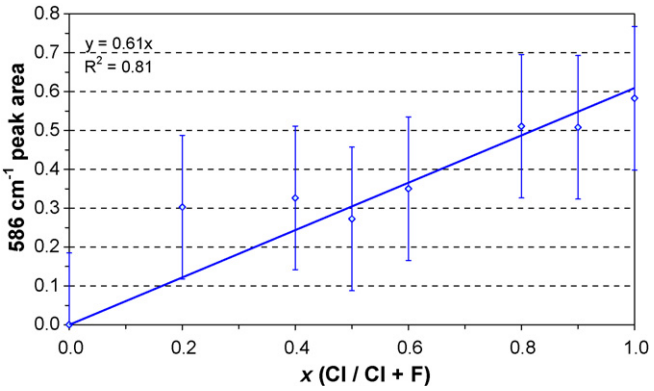

Fig. 3. 586 cm^{-1} peak area from ν_4 PO_4^{3-} band component in the series $Ca_5(PO_4)_3F_{1-x}Cl_x$.

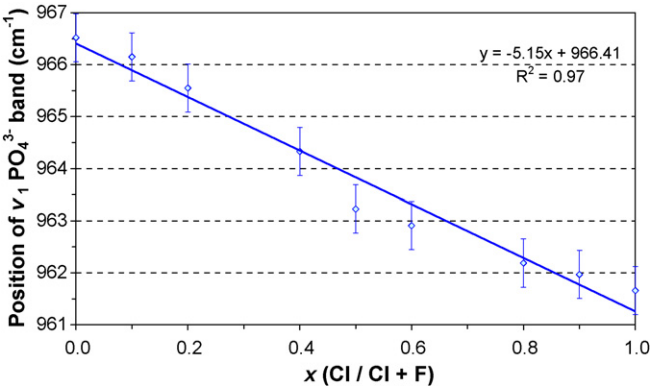

Fig. 5. Variation in ν_1 PO_4^{3-} band position for the series $Ca_5(PO_4)_3F_{1-x}Cl_x$.

3.1.2. 400–650 cm^{-1} region

Two bands can be seen in this region, the ν_2 band and the ν_4 band shown in Fig. 2. In hydroxyapatite we should see two bands due to the doubly degenerate ν_2 O–P–O bending mode and three bands for the triply degenerate ν_4 O–P–O bending mode.[21] Two components can be resolved in the ν_2 region for fluorapatite ($x = 0$): 431 and 447 cm^{-1}. These bands shift linearly to lower wavenumber with chlorine addition to 428 and 444 cm^{-1} on full substitution ($x = 1$). The ν_4 band shows four components for fluorapatite ($x = 0$): 582, 592, 608 and 617 cm^{-1}. These bands decrease linearly with chlorine addition to 577, 591, 613 and 619 cm^{-1} at $x = 1$. This region also develops an extra feature with chlorine addition, a band at 586 cm^{-1} for the pure chlorapatite ($x = 1$), not reported previously to our knowledge, however Elliot described a band at similar energy attributed to the E_g symmetry phonons in apatites.[22] This band follows the trend of shifting linearly to higher wavenumber with fluorine addition (to 591 cm^{-1} for $x = 0.2$) and was not present in fluorapatite ($x = 0.0$) or the $x = 0.1$ sample, although the signal is probably present but too weak to resolve the Lorentzian feature in the later sample. The area of this band increases linearly with chlorine addition as shown in Fig. 3, indicating this feature arises due to the influence of chlorine on the phosphate vibrational modes.

3.1.3. 940–990 cm^{-1} region

The position of the main phosphate band (ν_1) at around 966 cm^{-1} for fluorapatite ($x = 0.0$) seen in Fig. 4 decreases linearly with chlorine addition to 961 cm^{-1} for $x = 1.0$, depicted in Fig. 5 as predicted from Eq. (2). This band is a result of the non-degenerate P–O symmetric stretching mode.[21] The full-width half maximum (FWHM) of the ν_1 bands was obtained for all samples using Lorentzian deconvolution and is plotted against chlorine content in Fig. 6. It can be clearly seen that the width of this band increases with chlorine addition to the apatite. This indicates disordering of the structure with chlorine addition as an increase in peak width indicates a larger distribution of phosphate structural environments. This is not surprising as chlorine substitutes onto a different crystallographic site to fluorine, and local disorder in binary and ternary apatites results in a macroscopic space group which is not seen at the unit cell level.[10,18]

3.1.4. 1000–1100 cm^{-1} region

The ν_3 phosphate Raman spectral region can be seen plotted in Fig. 7. In hydroxyapatite we would expect three bands: due to the triply degenerate antisymmetric P–O stretching modes.[21] Five components were resolved using Lorentzian deconvolution, summarised in Table 1. For fluorapatite ($x = 0.0$) these bands

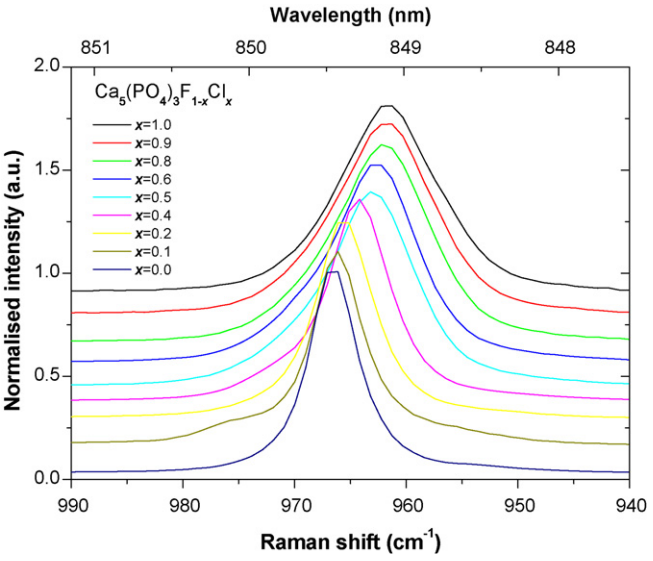

Fig. 4. Raman spectra of ν_1 PO_4^{3-} band in the series $Ca_5(PO_4)_3F_{1-x}Cl_x$.

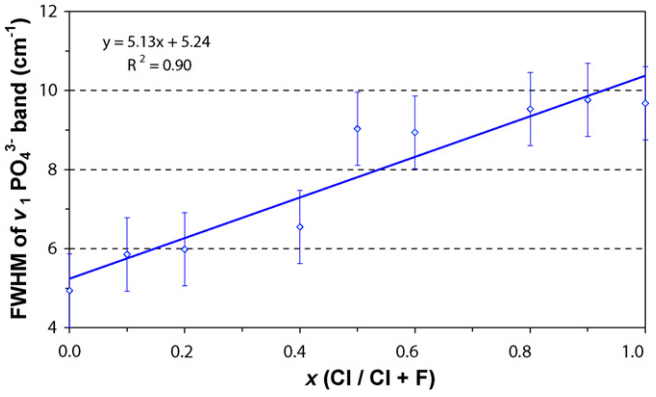

Fig. 6. Variation in ν_1 PO_4^{3-} band FWHM for the series $Ca_5(PO_4)_3F_{1-x}Cl_x$.

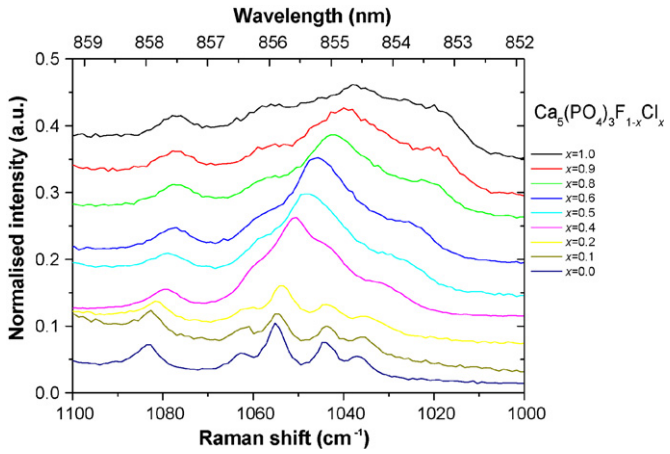

Fig. 7. Raman spectra of ν_3 PO_4^{3-} band in the series $Ca_5(PO_4)_3F_{1-x}Cl_x$.

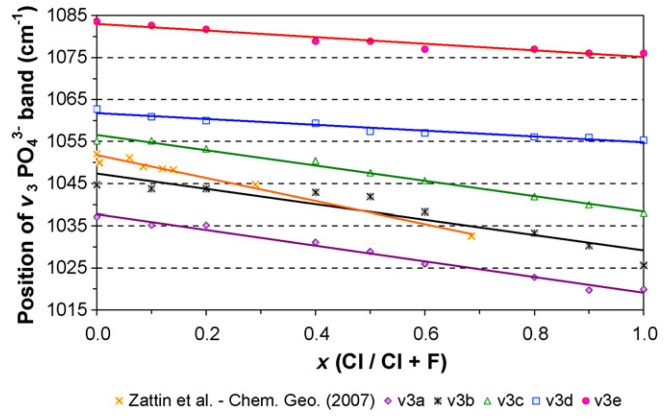

Fig. 8. Variation in ν_3 PO_4^{3-} band positions (five peaks) for the series $Ca_5(PO_4)_3F_{1-x}Cl_x$ compared to literature data.[23]

were seen at 1037, 1045, 1055, 1063 and 1084 cm^{-1}. The bands shifted linearly to lower wavenumber and were seen at 1020, 1026, 1038, 1055 and 1076 cm^{-1} for chlorapatite ($x = 1.0$). Zattin et al. using one of the ν_3 components to correlate the band position to chlorine content in geological apatites.[23] The variation in the position of all five ν_3 bands from this study can be seen plotted in Fig. 8 with the data from Zattin et al. for comparison. The values correlate quite well with the band around 1045 cm^{-1} for fluorapatite ($x = 0.0$), which is second highest in intensity. The band Zattin et al.[23] measured could have been the highest intensity component seen here at about 1055 cm^{-1} for a pure fluorapatite ($x = 0.0$), but the geological apatites measured[23] could have contained impurities such as hydroxyl groups and cations such as magnesium which would shift the Raman modes from the values seen here in the pure compounds.

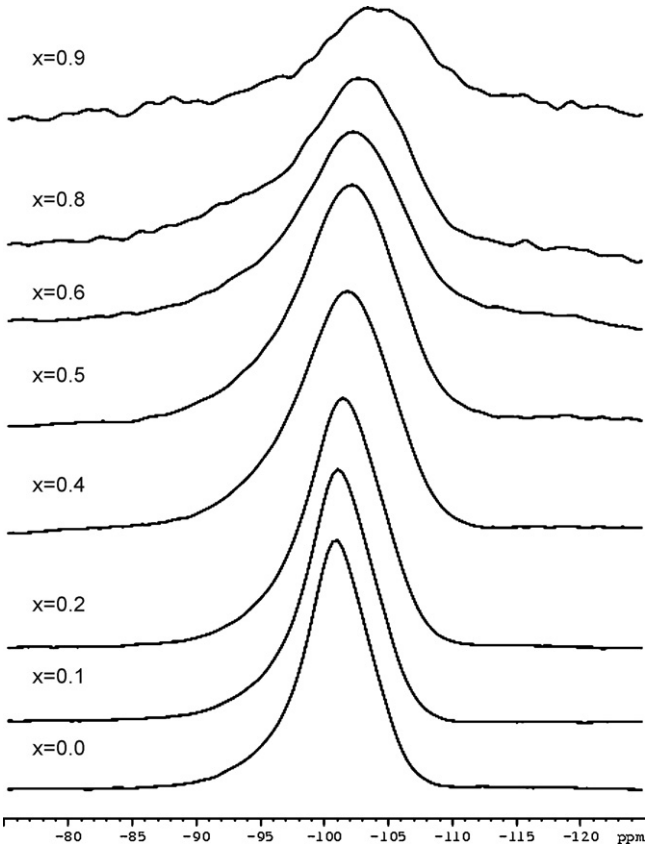

Fig. 9. ^{19}F MAS-NMR spectra of the series $Ca_5(PO_4)_3F_{1-x}Cl_x$.

3.2. NMR

3.2.1. ^{19}F

Fig. 9 shows the fluorine chemical shift moves upfield and FWHM increases linearly with chlorine content. This indicates the fluorine nuclei are on average becoming more shielded, as expected on addition of a less electronegative element (chlorine) to the apatite lattice. The peak broadening is a result of crystallographic disorder also seen in the Raman data. The ^{19}F resonance does not appear to develop any major asymmetry across the

Table 2
Position (δ), FWHM (w), in ppm, and fractional areas (f) of NMR peaks for the series $Ca_5(PO_4)_3F_{1-x}Cl_x$, N/A indicates no peak present

Cl (x)	^{19}F δ	^{19}F w	^{31}P δ_1	^{31}P w_1	^{31}P f_1	^{31}P δ_2	^{31}P w_2	^{31}P f_2	^{31}P δ_3	^{31}P w_3	^{31}P f_3
0.0	−102.8	5.3	N/A	N/A	N/A	3.3	0.9	1.00	N/A	N/A	N/A
0.1	−102.8	5.3	N/A	N/A	N/A	3.4	0.9	1.00	N/A	N/A	N/A
0.2	−103.1	5.9	1.8	0.9	0.06	3.4	1.0	0.94	N/A	N/A	N/A
0.4	−103.8	7.2	2.1	1.2	0.16	3.7	1.2	0.84	N/A	N/A	N/A
0.5	−103.4	7.5	2.5	1.5	0.31	3.8	1.2	0.69	N/A	N/A	N/A
0.6	−104.0	8.4	2.2	1.3	0.20	3.6	1.5	0.80	N/A	N/A	N/A
0.8	−105.2	8.3	1.9	0.9	0.06	3.4	1.0	0.94	N/A	N/A	N/A
0.9	−105.4	8.5	N/A	N/A	N/A	2.9	1.5	0.75	4.0	1.5	0.25
1.0	N/A	N/A	N/A	N/A	N/A	2.7	1.2	0.84	4.0	0.8	0.16

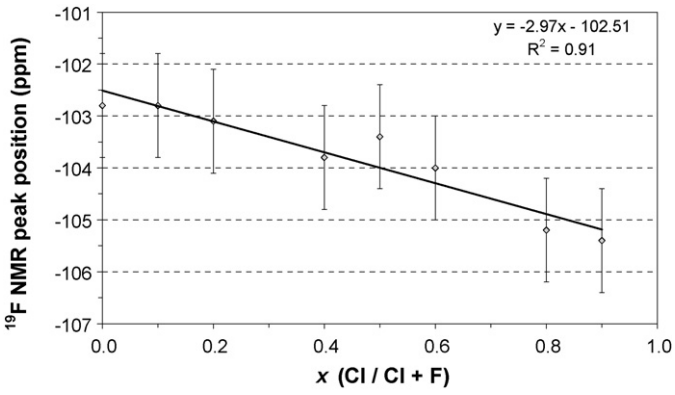

Fig. 10. Variation in ^{19}F MAS-NMR peak position for the series $Ca_5(PO_4)_3F_{1-x}Cl_x$.

series. The ^{19}F peak positions and widths are summarised in Table 2 and are also plotted in Figs. 10 and 11, respectively.

3.2.2. ^{31}P

As a general observation, the ^{31}P peak maximum (at around 3.3 ppm for fluorapatite, $x=0$[24,25]) initially shifts downfield to higher ppm values (3.8 ppm for $x=0.5$) then upfield for compositions where $x>0.5$ (2.7 ppm for $x=1$) indicating maximum deshielding occurs when the fluorine to chlorine ratio is approximately 1:1. For $x \geq 0.2$ a shoulder has developed (around 1.8 ppm) on the upfield side of the main peak. Like the main peak, this peak also increases to a maximum at $x=0.5$ (2.5 ppm) then decreases again to 1.9 ppm for $x=0.8$ and is not present for $x>0.8$. By $x \geq 0.9$ another prominent shoulder can be seen on the downfield side of the main fluorapatite peak at around 4.0 ppm for $x=0.9$ and 1.0.

A peak at around 1 ppm in biological apatites has been identified as surface 'acidic phosphate' groups—HPO_4^{2-}.[26] However, more recent studies,[27] in particular Jarlbring et al.,[28] used ^{31}P CP (cross-polarisation) NMR spectroscopy to distinguish between bulk and surface sites in synthetic fluorapatites. In addition to the main peak at around 2.9 ppm, assigned to bulk PO_4^{3-} groups, peaks at 0.8 and 5.4 ppm were seen. These were attributed to surface $\equiv PO_xH$ and surface $\equiv PO_x$.[28] From the data

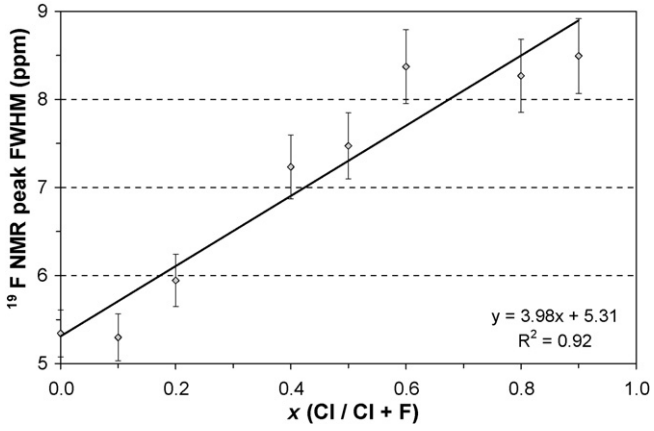

Fig. 11. Variation in ^{19}F MAS-NMR peak FWHM for the series $Ca_5(PO_4)_3F_{1-x}Cl_x$.

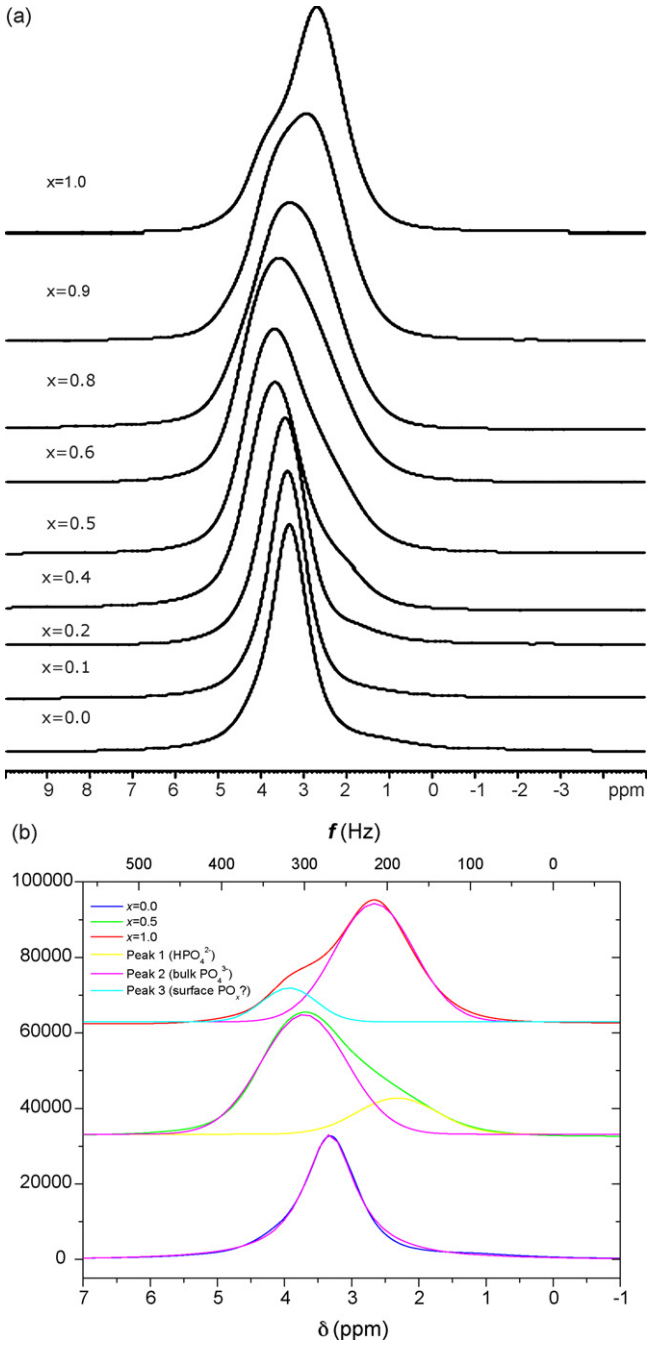

Fig. 12. (a) ^{31}P MAS-NMR spectra of the series $Ca_5(PO_4)_3F_{1-x}Cl_x$ and (b) with Gaussian deconvolution of selected compositions.

in Fig. 12 it can be seen even in the compositions $0.2 \leq x \leq 0.8$ there is a small peak which can be attributed to hydrolysed phosphate groups at around 2 ppm.[26–29] Another hypothesis could be that this peak has arisen due to phosphate groups in close proximity in chlorine rich ion channels, as the Raman band possibly due symmetry breaking (hexagonal to monoclinic) to was identified at $x=0.2$. This peak area increases to a maximum at $x=0.5$. In terms of thermodynamic stability, the $x=0.5$ composition is the most disordered and will hence be more susceptible to chemical degradation (i.e. hydrolysis of the smaller crystallites). The shoulder around 4 ppm in the chlorine rich compositions

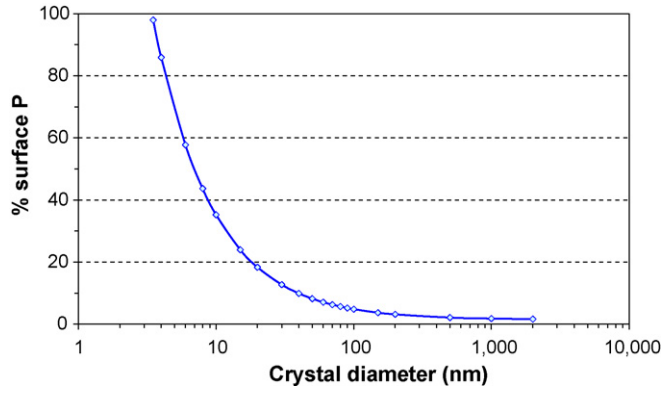

Fig. 13. Effect of crystallite size (for a fixed crystal length of 100 nm) on the amount of surface phosphate groups in chlorapatite.

could be due to surface $\equiv PO_x$ groups indicating a higher specific surface area in these samples.[27,28]

As these samples ($x \geq 0.9$) appear more disordered from the Raman data this peak at 4 ppm could be a result of increased phosphate groups at the small crystallite surfaces. For chlorapatite crystals 100 nm in length with 10 nm hexagon sides, we can calculated that around 18% of the phosphorus is present as surface groups, which is close to the values in Table 2 for the contribution of the 4 ppm peak. Fig. 13 illustrates the effect of crystallite size (variation in crystal diameter for a fixed crystal length of 100 nm) on the amount of surface phosphate groups in chlorapatite, which increases markedly for crystals smaller than around 100 nm. SEM micrographs of the fluorapatite sample ($x = 0$) showed crystallites to be in the order of 1 μm and at this size scale less than 0.5% of the phosphorus is present at the surface explaining the absence of the 4 ppm peak in this sample.

Raman indicated increased overall structural disorder with chlorine content (or possibly some ordering in the ion channels), which could arise from smaller crystals and hence increased phosphate sites at grain boundaries. The peaks related to phosphate groups in the bulk of the apatites: PO_4^{3-} at 3 ppm and HPO_4^{2-} at 2 ppm, show maximum peak broadening (FWHM in Table 2) around $x = 0.5$. NMR is far more sensitive to local disorder and the overall disorder seen by Raman and ^{19}F NMR is dominated by structural variations in the *c*-axis anion channels and increases with chlorine content. However, ^{31}P NMR shows us maximum disorder in terms of the number of spectral features in the local phosphorus environment at around $x = 0.5$ and the regular orthophosphate environment is possibly perturbed by increased hydrolysis of the material at this point as a result of the highest amount of HPO_4^{2-}: 31% from Table 2. The ^{31}P peak positions can be found summarised in Table 2 and plotted in Fig. 14.

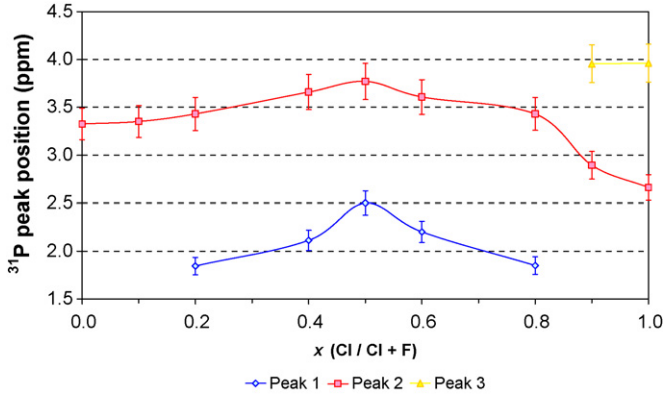

Fig. 14. Variation in ^{31}P MAS-NMR main peak position for the series $Ca_5(PO_4)_3F_{1-x}Cl_x$.

4. Conclusions

A complete series of fluorochloroapatites were synthesised and characterised using Raman spectroscopy. All Raman bands shifted to lower wavenumber with chlorine addition and peak widths increased indicating bulk structural disordering, as chlorine resides on a different crystallographic site to fluorine, or possibly some ordering in the *c*-axis ion channels. Raman spectroscopy is a powerful non-destructive tool which can be used to monitor chemical and structural changes in geological, biological, optical and nuclear materials. For example, the Raman band position of the ν_1 vibration could be used to accurately monitor the uptake of radioactive isotopes in waste streams such as ^{36}Cl or ^{90}Sr[30] *in situ* with a fibreoptic probe. The NMR peak position and width of the ^{19}F resonance shifted linearly with chlorine addition, decreasing and increasing, respectively consistent with fluorine disorder. However the ^{31}P spectra showed more complex behaviour, with multiple peaks present, indicating a possible structural transition (e.g. order ↔ disorder or monoclinic ↔ hexagonal) around the $x = 0.5$ composition, most likely short-scale phosphate disordering (e.g. higher HPO_4^{2-} content, halide ion channel ordering) at this point.

References

1. Ohtsuki, C., Kokubo, T. and Yamamuro, T., Mechanism of apatite formation on CaO–SiO_2–P_2O_5 glasses in a simulated body-fluid. *Journal of Non-Crystalline Solids*, 1992, **143**(May), 84–92.
2. Constantz, B. R., Ison, I. C., Fulmer, M. T., Poser, R. D., Smith, S. T., VanWagoner, M. *et al.*, Skeletal repair by *in situ* formation of the mineral phase of bone. *Science*, 1995, **267**(March), 1796–1799.
3. Penel, G., Leroy, G., Rey, C. and Bres, E., MicroRaman spectral study of the PO_4 and CO_3 vibrational modes in synthetic and biological apatites. *Calcified Tissue International*, 1998, **63**, 475–481.
4. Gallagher, K., Evolving temperature histories from apatite fission-track data. *Earth and Planetary Science Letters*, 1995, **136**, 421–435.
5. Deloach, L. D., Payne, S. A., Smith, L. K., Kway, W. L. and Krupke, W. F., Laser and spectroscopic properties of $Sr_5(PO_4)_3F$–Yb. *Journal of the Optical Society of America B: Optical Physics*, 1994, **11**(February), 269–276.
6. Bolland, M. D. A. and Bowden, J. W., The initial and residual value for subterranean clover of phosphorus from crandallite rock phosphates, apatite rock phosphates and superphosphate. *Nutrient Cycling in Agroecosystems*, 1984, **5**, 295–307.
7. Pappalardo, R. G., Walsh, J. and Hunt Jr., R. B., Cerium-activated halophosphate phosphors. *Journal of The Electrochemical Society*, 1983, **130**, 2087–2096.
8. Ma, Q. Y., Traina, S. J., Logan, T. J. and Ryan, J. A., *In situ* lead immobilization by apatite. *Environmental Science & Technology*, 1993, **27**(September), 1803–1810.

9. Metcalfe, B. L. and Donald, I. W., Candidate wasteforms for the immobilization of chloride-containing radioactive waste. *Journal of Non-Crystalline Solids*, 2004, **348**, 225–229.
10. Leroy, N. and Bres, E., Structure and substitutions in fluorapatite. *European Cells and Materials*, 2001, **2**, 36–48.
11. Jaffe, H. W., *Crystal Chemistry and Refractivity*. Dover, Mineola, 1996.
12. Greenwood, N. N. and Earnshaw, A., *Chemistry of the Elements*. Butterworth-Heinemann, Oxford, 1995.
13. Mackie, P. E., Elliot, J. C. and Young, R. A., Monoclinic structure of synthetic $Ca_5(PO_4)_3Cl$, chlorapatite. *Acta Crystallographica B*, 1972, **28**, 1840–1848.
14. Sudarsanan, K. and Young, R. A., Structural interactions of F, Cl and OH in Apatites. *Acta Crystallographica Section B: Structural Science*, 1978, **34**, 1401–1407.
15. Mackie, P. E. and Young, R. A., Fluorine–chlorine interaction in fluorchlorapatite. *Journal of Solid-State Chemistry*, 1974, **11**, 319–329.
16. Hughes, J. M., Cameron, M. and Crowley, K. D., Crystal-structures of natural ternary apatites—solid–solution in the $Ca_5(PO_4)_3X$ (X = F, OH, Cl) system. *American Mineralogist*, 1990, **75**(March–April), 295–304.
17. Hughes, J. M., Cameron, M. and Crowley, K. D., Structural variations in natural F, OH, and Cl apatites. *American Mineralogist*, 1989, **74**(July–August), 870–876.
18. McCubbin, F. M., Mason, H. E., Park, H., Phillips, B. L., Parise, J. B., Nekvasil, H. *et al.*, Synthesis and characterization of low–OH fluor-chlorapatite—a single-crystal XRD and NMR spectroscopic study. *American Mineralogist*, 2008, **93**(January), 210–216.
19. Penel, G., Leroy, G., Rey, C., Sombret, B., Huvenne, J. P. and Bres, E., Infrared and Raman microspectrometry study of fluor-fluor-hydroxy and hydroxy-apatite powders. *Journal of Materials Science-Materials in Medicine*, 1997, **8**(May), 271–276.
20. Kerr, J. A., *CRC Handbook of Chemistry and Physics* (*81 ed.*). CRC Press, Florida, 2000.
21. Fowler, B. O., Infrared studies of apatites. I. Vibrational assignments for calcium, strontium, and barium hydroxyapatites utilizing isotopic substitution. *Inorganic Chemistry*, 1974, **13**, 194–207.
22. Elliott, J. C., *Structure and chemistry of the apatites and other calcium orthophosphates*. Elsevier, Amsterdam, The Netherlands/New York, 1994.
23. Zattin, M., Bersani, D. and Carter, A., Raman microspectroscopy—a non-destructive tool for routine calibration of apatite crystallographic structure for fission-track analyses. *Chemical Geology*, 2007, **240**(June), 197–204.
24. Braun, M., Hartmann, P. and Jana, C., ^{19}F and ^{31}P NMR spectroscopy of calcium apatites. *Journal of Materials Science-Materials in Medicine*, 1995, **6**, 150–154.
25. Braun, M. and Jana, C., ^{19}F NMR spectroscopy of fluoridated apatites. *Chemical Physics Letters*, 1995, **245**, 19–22.
26. Wu, Y., Glimcher, M. J., Rey, C. and Ackerman, J. L., A unique protonated phosphate group in bone mineral not present in synthetic calcium phosphates: identification by phosphorus-31 solid-state NMR spectroscopy. *Journal of Molecular Biology*, 1994, **244**, 423–435.
27. Kolmas, J., Slosarczyk, A., Wojtowicz, A. and Kolodziejski, W., Estimation of the specific surface area of apatites in human mineralized tissues using ^{31}P MAS-NMR. *Solid-State Nuclear Magnetic Resonance*, 2007, **32**, 53–58.
28. Jarlbring, M., Sandstrom, D. E., Antzutkin, O. N. and Forsling, W., Characterization of active phosphorus surface sites at synthetic carbonate-free fluorapatite using single-pulse ^{31}P, and ^{31}P CP MAS-NMR. *Langmuir*, 2006, **22**, 4787–4792.
29. Roberts, J., Heughebaert, M., Heughebaert, J.-C., Bonar, L., Glimcher, M. and Griffin, R., Solid-state ^{31}P NMR studies of the conversion of amorphous tricalcium phosphate to apatitic tricalcium phosphate. *Calcified Tissue International*, 1991, **49**, 378–382.
30. O'Donnell, M. D., Fredholm, Y., de Rouffignac, A. and Hill, R. G., Structural analysis of a series of strontium substituted apatites. *Acta Biomaterialia*, 2008, **4**, 1455–1464.